# Spin-orbit coupling induced broadening of the spin crossover transition in divalent cobalt probed by $K_{\beta}$ x-ray emission

Michel van Veenendaal , <sup>1,2</sup> E. H. T. Poldi , <sup>3,2</sup> and Daniel Haskel <sup>2</sup>

<sup>1</sup>Department of Physics, Northern Illinois University, DeKalb, Illinois 60115, USA

<sup>2</sup>Advanced Photon Source, Argonne National Laboratory, 9700 South Cass Avenue, Argonne, Illinois 60439, USA

<sup>3</sup>Department of Physics, University of Illinois at Chicago, Chicago, Illinois 60607, USA

(Received 28 July 2025; accepted 3 October 2025; published 16 October 2025)

The pressure-induced spin crossover in divalent cobalt is studied. It is shown that the change in spin as a function of pressure and its effects on  $K_{\beta}$  x-ray emission depend on the 3d spin-orbit interaction and local exchange fields, leading to a broadening of the spin-crossover transition as a function of octahedral crystal field or pressure. A detailed comparison is made with experimental data on Na<sub>3</sub>Co<sub>2</sub>SbO<sub>6</sub> as a function of the octahedral field tuned by pressure. Additionally, the spectral weight of the  $K_{\beta'}$  feature is studied for transition metals, and the Tsutsumi rules [K. Tsutsumi, J. Phys. Soc. Jpn. 14, 1696 (1959); K. Tsutsumi and H. Nakamori, J. Phys. Soc. Jpn. 25, 1418 (1968); K. Tsutsumi *et al.*, Phys. Rev. B 13, 929 (1976)] are reexamined.

DOI: 10.1103/gwr2-txdy

#### I. INTRODUCTION

A spin crossover indicates a change in the local spin of, typically, a transition-metal ion [1,2]. Spin crossovers have potential applications in nanophotonic devices [3]. Examples are memory storage [1,2] and temperature-sensitive MRI contrast agents [4]. In many systems, the different spin states are clearly distinct configurations that are weakly coupled by the spin-orbit interaction, which can only change the spin S by  $\pm 1$  via the  $L_{\pm 1}S_{\pm 1}$  terms. In the prototypical spin crossover in  $d^6$  systems (Fe<sup>2+</sup> or Co<sup>3+</sup>), the spin changes from S=2 to S = 0. This requires two spin flips from S = 2 to 1 and from S = 1 to 0. The double spin flip makes the transition between the spin states far from trivial; see [5] and references therein. Due to the weak coupling, one expects a sharp transition between the spin states when, for example, the spin crossover is induced by pressure. This was clearly demonstrated by Weis et al. [6] who observed an extremely sharp transition for divalent iron. They also showed how a broadening of the transition can occur due to the coexistence of different spin states resulting from the pressure gradient due to the pressure medium that is used. The high-to-low spin transition can also be broad if the local moments are gradually destroyed in the competition between the increased bandwidth and the local spin formation due to the Coulomb interaction [7]. However, this is a continuous process over a very wide pressure range.

Recent pressure experiments [8] on divalent cobalt in Na<sub>3</sub>Co<sub>2</sub>SbO<sub>6</sub> only show a modest reduction due to the increased bandwidths up to the spin-crossover transition. This system was a candidate for a Kitaev spin liquid [9]. However, the material undergoes a spin crossover as a function of pressure which quenches the orbital degrees of freedom required for bond-directional exchange at the root of Kitaev's model. For this system, the spin transition as a function of pressure shows a substantial broadening. In this paper, it is demonstrated that this broadening is an intrinsic effect resulting from

the coupling of the high- and low-spin states via the spin-orbit interaction. Unlike  $\text{Co}^{3+}$ , where the spin crossover involves two spin flips, the spin transition in divalent cobalt  $(3d^7)$  is due to a single spin flip from  $t_{2g}^5 e_g^2$  (with total spin  $S = \frac{3}{2}$ ) to  $t_{2g}^6 e_g^1$  ( $S = \frac{1}{2}$ ). This leads to a stronger coupling between the high- and low-spin configurations, which makes the spin crossover significantly more interesting.

The spin crossovers are studied with  $K_{\beta}$  x-ray emission spectroscopy (XES), where the radiative  $3p \rightarrow 1s$  decay following the removal of a strongly bound 1s core electron is studied [10,11]. Isotropic  $K_{\beta}$  XES, i.e., spectra in the absence of polarization effects, is relatively insensitive to ground-state properties compared to, say, x-ray absorption. This is because the radiative transitions do not directly involve the valence shell and the ground-state properties are observed via interactions between the 3p core hole and the 3d valence electrons. The spectral line shape is dominated by the strong 3p-3dCoulomb interaction and a large core-hole lifetime broadening. This allows one to probe the total spin S of the valence shell, but provides little insight into, say, the magnitude of local crystal fields or any orbital effects. More sensitivity can be obtained by using polarization effects. This can be done in the excitation process by leveraging the spin selectivity of XES to probe the spin splitting of the empty density of states with spin-selective x-ray absorption measurements [12–15]. Alternatively, dichroism in the x-ray emission process can be measured [16]. However, in the study of spin crossovers, isotropic nonresonant  $K_{\beta}$  XES is often preferred over, for example, L-edge x-ray absorption spectroscopy (XAS) since hard x-rays have the advantage over soft x-rays that they do not require ultrahigh vacuum and that they can penetrate a diamond anvil pressure cell. Spin crossovers can be studied theoretically by a variety of different methods. Our interest lies in the transition as a function of pressure. Due to the difference in spin, one could expect the spin transition to be sharp as a function of pressure. However, experimentally, this is generally not the case. Theoretically, a broad transition between the high- and low-spin states as a function of pressure has been obtained in dynamical mean-field studies of MnO [7], where a gradual spin crossover is obtained by a reduction in the Coulomb exchange when the volume of the system decreases. Combined with the change in crystal field, this lowers the energy of the spin-down  $t_{2g}$  band and increases the energy of the spin-up  $e_g$  band. This causes the  $e_g$  electrons to be transferred into the  $t_{2g}$  down-spin states. Since the bandwidths are several electronvolts wide, this transition is smooth as a function of pressure. In recent experiments on divalent cobalt [8], the local spin only shows a modest reduction up to the spin-crossover transition. This transition is studied in a local model that has a spin-crossover transition without a significant reduction of the Coulomb exchange. This allows additional interactions, such as the spin-orbit interaction in combination with exchange fields, to affect the spin states. This leads to a more complex spin-crossover transition.

It is shown that these effects are visible in  $K_{\beta}$  emission, leading to a broadening of the transition that is dependent on the coupling between the spin states. The paper is divided as follows. In Sec. II, the model used in the calculations is described. In Sec. III, we take a closer look at how  $K_{\beta}$  XES is sensitive to the local spin and look into more detail at the spectral weights and reexamine the rules given by Tsutsumi *et al.* [17–19]. In Sec. IV, the focus then shifts to the pressure-induced spin crossover in divalent cobalt. It is demonstrated how relatively small parameters, such as the spin-orbit interaction and local exchange fields, can affect the pressure dependence of the spin crossover.

#### II. MODEL

The  $K_{\beta}$  XES spectra are calculated using ionic models including the full Coulomb multiplet interaction [20–22]. The parameters for the Coulomb and spin-orbit interactions are calculated within the Hartree-Fock limit [23]. The crystal field is an adjustable parameter that simulates the change in the local octahedral surroundings. The crystal field strength 10Dq is 1.1 eV at ambient pressure, which was obtained from a detailed fit of the L-edge x-ray absorption [22]. A crystal field of 2.3 eV is needed to induce a crossover from high-to-low spin.

The spectra are calculated using [14]

$$I(\omega') = \sum_{f} |\langle f|D|\underline{1s}\,g\rangle|^2 \delta(\hbar\omega' + E_f - \varepsilon_{1s} - E_g), \quad (1)$$

where  $\hbar\omega'$  is the energy of the emitted photon,  $E_f$  and  $E_g$  are the final and ground-state energies, respectively,  $\varepsilon_{1s}$  is the binding energy of the 1s electron, and D is the dipole operator. This assumes that the initial photoexcitation of the 1s electron has only a minor effect on the nature of the ground state. This is a good approximation since the Coulomb exchange between the 1s and 3d electrons is small with the Coulomb exchange parameter [21] equal to  $F^2=65$  meV. Since this is significantly smaller than the 1s core-hole lifetime broadening (1.2 eV FWHM), all intermediate states contribute to the emission process.

#### III. THE S/(S+1) INTENSITY RATIO RULE

The experimental  $K_{\beta}$  x-ray emission spectra are relatively simple due to the lifetime broadening of several electronvolts of the 3p core hole. They are often characterized by a strong main peak denoted as  $K_{\beta_{1,3}}$  and a weaker feature, generally denoted by  $K_{\beta'}$ , at lower outgoing photon energies. Since the excitation and emission processes do not directly involve the 3d valence shell, the spectral line is relatively insensitive to ground-state properties such as the projected orbital and spin moments. However, it is sensitive to the total spin moment since the spectral features are largely due to the strong Coulomb interaction between the 3p core level and the 3d valence shell. The sensitivity of the  $K_{\beta}$  x-ray emission to the total spin in the ground state S makes it a useful tool in the study of spin-crossover phenomena.

The analytical understanding of the  $K_{\beta}$  intensities has, for a long time, been dominated by the rules given by Tsutsumi *et al.* [17–19]. When neglecting the spin-orbit interaction, the states are defined by their total spin. Since the radiative transitions do not include the valence shell, the probability of reaching a certain final-state total spin is determined by the degeneracy of the spin state. When the spin carried by the valence electrons in the ground state is S, the possible final-state spins are  $S_{\pm} = S \pm \frac{1}{2}$ , with the  $\pm$  indicating the orientation of the 3p spin relative to the valence spin. The relative intensities of reaching final states with  $S_{\pm}$  is then given by

$$\frac{I_{S_{-}}}{I_{S_{-}}} = \frac{[S_{-}]}{[S_{+}]} = \frac{2S_{-} + 1}{2S_{+} + 1} = \frac{S}{S + 1},\tag{2}$$

where the shorthand for the multiplicity [S] = 2S + 1 is used. The multiplicity arises from the number of projected spin components,  $M_S = S, S - 1, \ldots, -S$ .

The additional assumption [17–19] is that the  $K_{\beta_{1,3}}$  and  $K_{\beta'}$  are separated by an energy J(S+1), where J is the effective Coulomb exchange between the 3p hole and the 3d electrons. However, whereas the intensity ratio rule is exact, the identification of  $K_{\beta_{1,3}}$  and  $K_{\beta'}$  with  $S_+$  and  $S_-$ , respectively, is not. Although  $K_{\beta'}$  has predominantly  $S_-$  character, the main  $K_{\beta_{1,3}}$  also has a significant contribution from  $S_-$  states, as the calculations below will show.

To elucidate the deviation of experimental observations from Tsutsumi's rule, spectra are calculated in spherical or SO(3) symmetry in the absence of spin-orbit interaction. Although the spin-orbit coupling strength  $\zeta_{3p} = 1.14 \,\text{eV}$  is not negligibly small, the spectral features of the  $K_{\beta}$  spectra are dominated by the Coulomb interactions that spread out the spectral features over 15–20 eV. Focusing solely on the Coulomb interactions allows the identification of the total spin and orbital moments in the different final states. The lifetime broadening is 2.5 eV FWHM. This lifetime broadening is less than the intrinsic value to make the spectral features more identifiable. Details given later in the paper show an energydependent broadening larger than 3.75 eV. Additionally, a Gaussian broadening of 1 eV was used to simulate experimental resolution. The spectra for different numbers of 3d electrons are given in Fig. 1. Although additional interactions can further split the final states, they are too small to cause a significant transfer of spectral weight between the  $K_{\beta_{1,3}}$  and

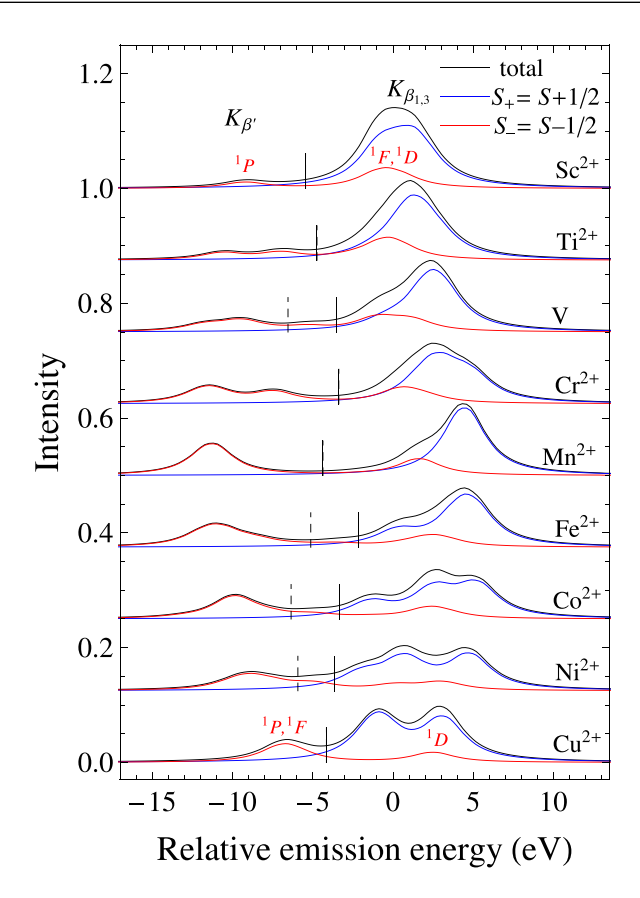


FIG. 1. The  $K_{\beta}$  spectra in spherical symmetry for divalent transition-metal ions from  $3d^1$  (Sc<sup>2+</sup>) to  $3d^9$  (Cu<sup>2+</sup>). The total  $K_{\beta}$  spectra (black) are divided into  $S_+$  (blue) and  $S_-$  (red) contributions. To avoid large shifts in energy, the spectra are plotted as a function of the relative emission energy such that the first moment of the spectrum is zero. The small vertical lines indicate the separation between the  $K_{\beta_{1,3}}$  and  $K_{\beta'}$  features. For the solid lines, there is no  $S_+$  contribution at lower emission energy. For some spectra, the  $K_{\beta_{1,3}}$  and  $K_{\beta'}$  are separated by the local minimum in the emission spectrum; see vertical dashed lines. For Sc<sup>2+</sup> and Cu<sup>2+</sup>, the composition of the spectra in terms of Coulomb multiplets is shown for the singlet states; see text.

 $K_{\beta'}$  regions. Therefore, they will not significantly affect the discussion of Tsutsumi's rules.

In the next section, we shall see that the 3d spin-orbit coupling can have an effect on the  $K_{\beta}$  emission spectra in divalent cobalt. This might seem surprising since the interaction strength  $\zeta_{3d}=66\,\mathrm{meV}$  is very small. However, the changes are not a result of final-state effects, but due to a change in the ground state. In the presence of the 3d spin-orbit coupling, the total spin S in the ground state is no longer a good quantum number. The mixing of different spin states is obviously particularly strong close to a spin crossover. This can have a strong effect on how the final states are accessed.

Let us look at the spectra in spherical symmetry; see Fig. 1. First of all, we note that the intensity ratio rule in Eq. (2) is correct for the calculated spectra. The ratio of the integrated intensities of the spectra with  $S_- = S - \frac{1}{2}$  (red lines) and  $S_+ = S + \frac{1}{2}$  (blue lines) final states (see Fig. 1) is indeed given by S/(S+1). However, whereas the  $K_{\beta'}$  is due to  $S_-$  final

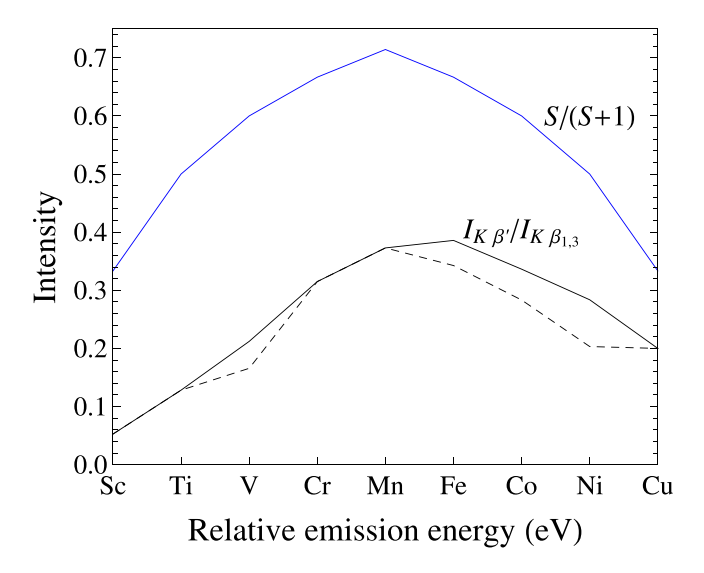


FIG. 2. The intensity ratio  $I_{K_{\beta'}}/I_{K_{\beta_{1,3}}}$  as a function of the number of 3d electrons indicated by the elements of the divalent ions. The solid and dashed lines give the intensity ratios for the different separations of  $K_{\beta'}$  and  $K_{\beta_{1,3}}$ ; see Fig. 1. For comparison, the blue line gives Tsutsumi *et al.*'s [17–19] estimate S/(S+1).

states,  $S_{-}$  spectral weight is also present in the main  $K_{\beta_{1,3}}$  region; see the red lines in Fig. 1.

The value of S/(S+1) therefore cannot be directly associated with the intensity ratio of  $K_{\beta'}$  and  $K_{\beta_{1,3}}$ . To determine the real intensity ratio, one must first define  $K_{\beta'}$ . Although still relatively straightforward in spherical symmetry, there is unfortunately no clear definition of the  $K_{\beta'}$  states and its identification becomes harder for more complicated systems including crystal fields and spin-orbit interactions. For spherical symmetry, the best definition is the  $S_{-}$  final states with an emission energy lower than the lowest  $S_+$  final states. This separation is given by the small solid vertical lines in Fig. 1. The intensities are calculated without applying the broadenings. Therefore, the tails of the  $S_+$  features can cross the solid vertical lines without affecting the theoretical calculations of the  $K_{\beta'}$ - $K_{\beta_1,3}$  intensity ratios. Although this identification is straightforward in a theoretical calculation, these emission energies can be rather close to the main  $K_{\beta_{1,3}}$  features. Experimentally, one might choose a different separation, for example, the minimum in the spectrum between  $K_{\beta'}$  and  $K_{\beta_1}$ . This is indicated by the small dashed vertical lines in Fig. 1.

After the identification of the  $K_{\beta'}$  region, the intensity ratio can be calculated; see Fig. 2. The intensity ratio is off by a factor 1.7–6.3 with the S/(S+1) estimate [17–19]. Surprisingly, although one might expect the S/(S+1) rule to work better for early transition metals due to the larger energy separation between  $K_{\beta'}$  and  $K_{\beta_{1,3}}$ , it is actually worse due to the significant  $S_-$  contributions to the main  $K_{\beta_{1,3}}$  line. Additionally, the difficulties in identifying the  $K_{\beta'}$  region can further decrease the agreement.

However, despite these limitations, the  $K_{\beta'}$  region still predominantly consists of  $S_-$  states. Therefore, it will show a sensitivity to a change in the ground-state total spin, which is one of the more interesting features of  $K_{\beta}$  emission. Additionally, the S/(S+1) rule provides a decent indication

of the relative trend of the  $K_{\beta'}$ - $K_{\beta_{1,3}}$  intensity ratio across the transition-metal series. However, one should be careful drawing too many conclusions from a semiquantitative analysis without an accompanying calculation of the spectral line shape.

Let us try to obtain a better understanding of the intensity ratios. When the outgoing polarization is not measured, the intensities can be determined by looking at the maximum spin since all spin directions give the same result. For a particular ground-state spin S due to the  $3d^n$  valence electrons and a core-level spin  $\sigma = \pm \frac{1}{2} = \uparrow, \downarrow$  parallel or antiparallel to S, the intensities to final states of a particular spin are given by

$$I_{\sigma}^{\pm} = \left| \left\langle S_{\pm}, S + \sigma \left| SS; \frac{1}{2}\sigma \right\rangle \right|^{2}, \tag{3}$$

where constant factors, such as reduced matrix elements, have been omitted;  $S_{\pm}=S\pm\frac{1}{2}$ ; and  $\langle JM|J_1M_1;J_2M_2\rangle$  is a Clebsch-Gordan coefficient that couples  $J_1$  and  $J_2$  to a total angular momentum J. When the spin of the core level is parallel to the valence spin, only final states with  $S_+=S+\frac{1}{2}$  can be reached and  $I_+^+=1$  and  $I_-^-=0$ . When the spin of the core level is antiparallel to the valence spin S, final-state spins  $S_-=S-\frac{1}{2}$  can be reached. However, it is still possible to reach the  $S_+$  final states with projected spin  $M_S=S-\frac{1}{2}=S_+-1$ . Their intensities are given by  $I_+^-=2S/[S]$  and  $I_+^+=1/[S]$ , using the shorthand [S]=2S+1. The dependence in reaching final-state spin values on the direction of the spin of the core level relative to the valence spin results in the spin sensitivity of the resonant XES spectra [14]. The ratio of reaching the  $S_\pm$  final states is then

$$\frac{I_{\downarrow}^{-}}{I_{\uparrow}^{+} + I_{\downarrow}^{+}} = \frac{2S/[S]}{1 + 1/[S]} = \frac{S}{S + 1}.$$
 (4)

This reproduces the Tsutsumi spin ratio in Eq. (2).

A similar analysis can be performed when looking at the orbital angular momenta. The probability of reaching a certain final state L' of the  $3p^53d^n$  configuration is given by

$$I_q^{L'} = |\langle L', L+q|LL; 1q \rangle|^2, \tag{5}$$

where q = 1, 0 - 1 is the polarization of the outgoing radiation. Again, if we are not measuring the polarization of the outgoing light, one can consider the maximum projected orbital angular momentum value  $M_L = L$  since all directions produce the same result. In the absence of polarization detection, the intensity for a particular final state L' = L + 1, L, L - 1 value is given by

$$I^{L'} = \sum_{q=-1}^{1} I_q^{L'} = \frac{[L']}{[L]}.$$
 (6)

As with the spin, the probability of reaching a particular L' value is simply given by the multiplicity of the final state. Note that the total intensity is independent of L,

$$I_{\text{tot}} = \frac{1}{3} \sum_{L'=L-1}^{L+1} I^{L'} = 1.$$
 (7)

This is expected since the  $3p \rightarrow 1s$  decay should be independent of the orbital angular momentum L of the valence shell.

Let us apply this to the simple cases of  $Cu^{2+}$  and  $Sc^{2+}$ . Both have the same final-state multiplets  ${}^{1,3}P$ ,  ${}^{1,3}D$ , and  ${}^{1,3}F$ using the notation  ${}^{2S+1}X$  with X = S, P, D, F, ... for total angular momenta L = 0, 1, 2, 3. These are the possible multiplets that can be formed by combining a 3p hole with orbital angular momentum  $l_{3n} = 1$  and a 3d electron or hole (for Sc<sup>2+</sup> and  $Cu^{2+}$ , respectively) with  $l_{3d} = 2$ . The total angular momenta are then  $L = l_{3p} + l_{3d}, \dots, |l_{3p} - l_{3d}| = 3, 2, 1$ . From a "spectroscopic" point of view, the systems are comparable since all the multiplets have the same intensities for scandium and copper. If one assumes the  $K_{\beta_{1,3}}$  and  $K_{\beta'}$  lines have only triplet and singlet character, then the intensity ratio would be given by  $I_{K_{\beta'}}/I_{K_{\beta_{1,3}}} = [S_-]m/[S_+]m = S/(S+1) = \frac{1}{3}$ , where the total orbital multiplicity is  $m = \sum_{L'=L-1}^{L+1} [L]$  and the spin multiplicity is  $[S_{\pm}] = 1, 3$  for  $S_{\pm} = 0, 1$ , respectively. These are the values given by the blue line in Fig. 2. For Cu<sup>2+</sup> and  $Sc^{2+}$ , the total orbital multiplicity is m = 15. Note that the total orbital multiplicity is equal to the total number of orbital states that can be made when combining a 3p and a 3d orbital, i.e.,  $3\times 5=15$ . Combined with the spin, there are a total of 60 possible states. The L and S quantum numbers indicate how the states split in the presence of Coulomb interactions. If the  $K_{\beta_{1,3}}$  and  $K_{\beta'}$  are solely determined by the spin  $S_{\pm}$ , then the total orbital multiplicity m cancels since all angular momentum values can be reached in both spectral

However, the spectra do not look the same (see Fig. 1) since the eigenenergies of the multiplets for  $3p^53d^1$  and  $3p^53d^9$ are different. This is because the Coulomb interaction is also strongly dependent on the orbital angular momentum L and the assumption that it is only determined by the final-state spin  $S_{\pm}$  is an oversimplification. As can be seen in Fig. 1, for both Sc and Cu, the  $K_{\beta_{1,3}}$  region contains singlet character. For copper, the singlet intensity in the  $K_{\beta_{1,3}}$  is due to the  ${}^{1}D$ multiplet. The  $K_{\beta'}$  region consists of  ${}^{1}P$  and  ${}^{1}F$  multiplets, whose energy separation is less than the lifetime broadening. When calculating the intensity ratio, the  ${}^{1}D$  intensity has to be included in the  $K_{\beta_{1,3}}$  region. This gives  $I_{K_{\beta'}}/I_{K_{\beta_{1,3}}}=$  $[S_{-}]([1] + [3])/([S_{+}]m + [S_{-}][2]) = \frac{1}{5} = 0.2$ , where [L] =2L + 1 are the multiplicities of the orbital angular momenta; see Fig. 2. For scandium, the  $K_{\beta'}$  intensity is even weaker since the only multiplet in this region is  ${}^{1}P$ . The intensity ratio is then given by  $I_{K_{\beta'}}/I_{K_{\beta_1,3}} = [S_-][1]/\{[S_+]m + [S_-]([2] + [S_+]m + [S_-])\}$ [3])} =  $\frac{1}{19} \cong 0.053$ , in agreement with Fig. 2.

The analysis becomes more complicated for other elements. For example, for Ni<sup>2+</sup>, the final states that can be reached from the  ${}^3F$  ground state are  ${}^{2,4}D$ ,  ${}^{2,4}F$ , and  ${}^{2,4}G$ . The  $K_{\beta'}$  region consists of  ${}^2D$  and  ${}^2G$  spectral weight;  ${}^2F$  intensity can be found close to the boundary between the  $K_{\beta_{1,3}}$  and  $K_{\beta'}$  features. Note that this division is a human definition based on the energies of the final states. There is nothing fundamental that clearly distinguishes the  $K_{\beta'}$  from  $K_{\beta_{1,3}}$  since the multiplets for different spins simply overlap. Although it appears that all doublet states are close to the  $K_{\beta'}$  region, there are additional multiplets with the same L and S values. For example,  ${}^2F$  occurs at energies -6.99, 0.39, and 3.34 eV with relative weights 0.047, 0.014, and 0.051, respectively; see Fig. 1. The latter two are clearly both in the  $K_{\beta_{1,3}}$  region.

The addition of spin-orbit and crystal-field interactions further complicates matters. However, these interactions are significantly smaller than the 3p-3d Coulomb exchange. In summary, although the  $K_{\beta'}-K_{\beta_{1,3}}$  intensity ratio is sensitive to changes in the ground-state spin S, not all  $S-\frac{1}{2}$  final states are in the  $K_{\beta'}$  region and interpretations of  $K_{\beta}$  XES should be accompanied by detailed calculations of the spectra.

#### IV. SPIN CROSSOVER IN DIVALENT COBALT

Although less commonly studied than spin crossovers in  $3d^6$  systems, divalent cobalt  $(3d^7)$  can also show a high-to-low spin transition as a function of increasing crystal field. This has become relevant recently when honeycomb systems, such as Na<sub>3</sub>Co<sub>2</sub>SbO<sub>6</sub>, were suggested as potential Kitaev spin-liquid systems [9]. Attempts have been made to push the system into the spin-liquid state by applying pressure. However, a high- to low-spin crossover removes the orbital degrees of freedom required for the bond-directional exchange anisotropy of Kitaev's model [8]. Here, we look in detail at the  $K_{\beta}$  emission for the spin crossover in divalent cobalt.

Let us first look at the spin crossover in more detail. Figure 3(a) shows the hole densities in the  $e_g$  and  $t_{2g}$  orbitals as a function of the octahedral crystal field 10Dq. Here, the focus is on the effects due to 10Dq. Additional small noncubic crystal fields, such as those arising from a trigonal distortion [22], are neglected. In the high-spin state, the irreducible representation of the ground state without spin-orbit coupling is  ${}^4T_1[t_{2g}^5e_g^2({}^3A_2)]$  and hole densities of  $\underline{n}_{e_g}=2$  and  $\underline{n}_{t_{2g}}=1$  are expected. For the low-spin state, the ground state is  $t_{2g}^6 e_g^1$  ( $^2E$ ) and  $\underline{n}_{e_o} = 3$  and  $\underline{n}_{t_{2o}} = 0$ . Away from the spin crossover, the hole densities are close to these values [see Fig. 3(a)], but on closer inspection, deviations from this simple picture occur. First, the hole densities in the high-spin state are  $\underline{n}_{e_p} \cong 1.95$ and  $\underline{n}_{t_{2\rho}} \cong 1.05$ . This is due to the Coulomb mixing with the  ${}^{4}T_{1}[(t_{2\rho}^{4}({}^{3}T_{1})e_{\rho}^{3}]$  state [22]. Similar small deviations due to Coulomb mixing are present for the low-spin state.

Second, although there is a discrete jump at the spincrossover point at  $10Dq = 2.268 \,\mathrm{eV}$ , the hole densities in the low-spin state change over several tenths of electronvolts to reach their asymptotic values. This should be contrasted with the high-spin state, where the hole densities are (almost) constant. However, in the presence of an exchange field due to neighboring spins,  $H_{\text{exch}} = \Delta_{\text{ex}} \sum_{m} \sigma d_{m\sigma}^{\dagger} d_{m\sigma}$ , where m = 2, 1, 0, -1, -2 is the projected angular momentum and  $\sigma = \pm \frac{1}{2}$  is the projected spin moment, the transition no longer shows a discrete jump. Note that long-range magnetic order is not needed for the lowering of the local symmetry. This behavior can be understood as follows. The different spin states are mixed by the 3d spin-orbit coupling. The orbital symmetry  $T_1$  can be viewed as an effective  $L_{\text{eff}} = 1$  state. Coupling with the  $S = \frac{3}{2}$  spin gives effective total angular momentum states  $J_{\text{eff}} = \frac{1}{2}, \frac{3}{2}, \frac{5}{2}$ , where the ground state has  $J_{\rm eff} = \frac{1}{2}$ . This picture is somewhat simplified [22]. It is more appropriate to use the E' and U' irreducible representations for octahedral symmetry [24], which are two- and fourfold degenerate, respectively. The  $J_{\rm eff}=\frac{1}{2}$  and  $\frac{3}{2}$  then become E' and U'. Within octahedral symmetry, the sixfold degenerate  $J_{\text{eff}} = \frac{5}{2}$  splits into  $E' \oplus U'$  [22]. The fourfold degenerate

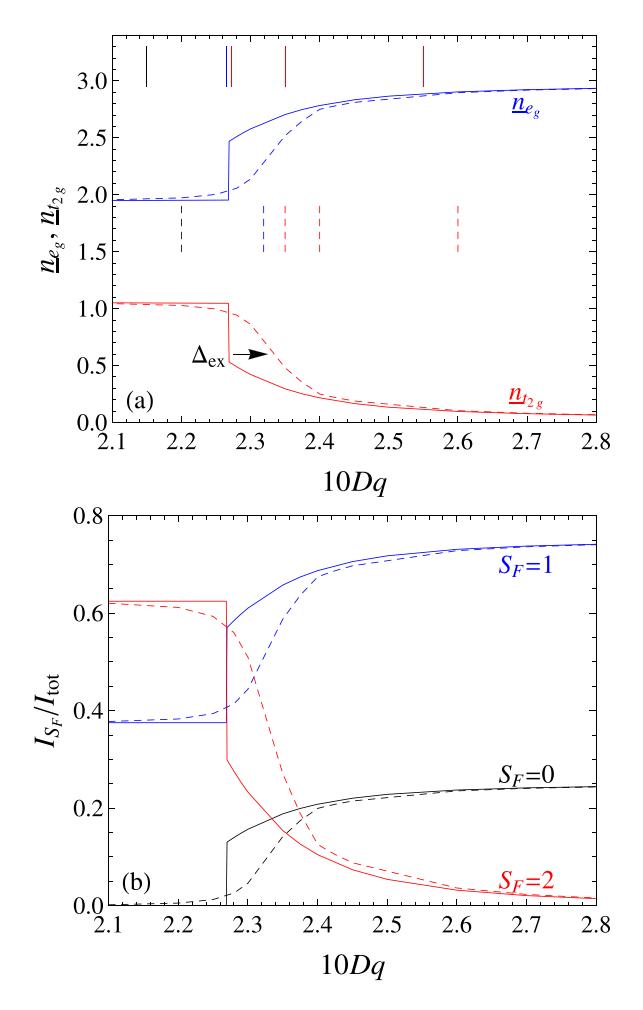


FIG. 3. (a) The hole densities  $\underline{n}_{e_g}$  and  $\underline{n}_{t_{2g}}$  as a function of the crystal field. The solid and dashed lines give the results without and with an exchange field  $\Delta_{\rm ex}=50\,{\rm meV}$  acting on the spins, respectively. The vertical lines indicate the 10Dq values for which the  $K_\beta$  x-ray emission is shown in Fig. 4. (b) The integrated intensities  $I_{S_F}$  separated by different final-state spins  $S_F$  normalized to the total integrated intensity  $I_{\rm tot}$  of the  $K_\beta$  emission.

low-spin state  ${}^{2}E$  becomes a U' irreducible representation when the orbital and spin are coupled.

For high-spin divalent cobalt, the ground state is  $E'(J_{\rm eff}=\frac{1}{2})$ . Since the spin-orbit interaction is a scalar, it can only couple states with the same irreducible representation. However, the low-spin state has a U' symmetry and therefore does not couple to the high-spin state below the high-to-low spin transition. Therefore, the hole densities are almost unaffected. Above the high-to-low spin crossover, the ground state is U' representing the low-spin state. Although U' does not couple to the lowest high-spin state, it does couple to the high-spin U' states (arising from  $J_{\rm eff}=\frac{3}{2},\frac{5}{2}$ ). This mixing of the low- and high-spin states causes the gradual change in the hole densities above the high-to-low spin crossover.

The discrete change in the hole densities entirely disappears when the symmetry is lowered by the presence of, say, an exchange field working on the spin. As a result, the fourfold degenerate low-spin state U' splits into two twofold degenerate states. These states now couple with the twofold degenerate high-spin ground state. The presence of the

exchange field now completely removes the jump in the spin crossover; see Fig. 3(a). The presence of the exchange field also increases the 10Dq value needed for a spin crossover by  $\Delta_{\rm ex}=50$  meV; see Fig. 3(a). The width of the transition is related to the spin-orbit coupling strength  $\zeta_{3d}=66$  meV in the ground state calculated within the Hartree-Fock limit [22,23], which is comparable to the change in 10Dq across the transition. Note that the effective spin-orbit coupling strength for the splitting of the  $^4T_1$  state is further reduced [22].

Figure 3(b) shows the integrated intensities  $I_S$  over the entire  $K_{\beta}$  XES spectrum for a particular final-state total spin  $S_F$  normalized to the total integrated intensity  $I_{\text{tot}}$ . This calculation is somewhat artificial since the final-state spin  $S_F$  is not a good quantum number in the presence of the 3d and 3p spin-orbit interactions. Additionally, the final-state crystal field is switched off to allow the identification of the different spin states. However, the purpose of this figure is to show how the spin-orbit coupling in the ground state affects how the final states of different spin are accessed, which can change the  $K_{\beta'}$  intensity. Since the integrated intensities are normalized to the total intensity, the expected integrated intensities  $I_S/I_{tot}$ are (S + 1)/(2S + 1) and S/(2S + 1) for  $S_F = S \pm \frac{1}{2}$ , respectively. In the high-spin state  $(S = \frac{3}{2})$ , one therefore expects  $\frac{5}{8} = 0.625$  and  $\frac{3}{8} = 0.375$  for  $S_F = 2$  and  $S_F = 1$ , respectively. For the low-spin state  $(S = \frac{1}{2})$ , the expected integrated intensities are  $\frac{3}{4} = 0.75$  and  $\frac{1}{4} = 0.25$  for  $S_F = 1$  and  $S_F = 0$ , respectively. These values are close to those in Fig. 3(b) when the system is far from the spin crossover.

The effect of the spin-orbit coupling in the ground state on the integrated intensities is comparable to what was observed for the hole densities. In the absence of an exchange field, the lowest high-spin state mixes little with the low-spin state and the values of  $I_{S_F}$  remain almost constant. When exceeding the critical crystal-field value, a sudden jump in integrated intensities occurs, followed by a slower decay of their asymptotic values; see Fig. 3(b). In the presence of an exchange field, mixing between high- and low-spin states occurs throughout and a smooth transition of the integrated intensities is found.

Let us now consider the effect of the changes in groundstate properties on the  $K_{\beta}$  emission. The spectra in the absence of an exchange field are given in Fig. 4(a). The XES spectra are calculated for the 10Dq values indicated by the solid vertical lines in Fig. 3(a). The lifetime broadening is reduced with respect to the intrinsic value to 2.5 eV FWHM to bring out the spectral features more clearly. Additionally, a Gaussian broadening of 1 eV was used to simulate experimental resolution. Since the high-spin ground state almost does not mix with the low-spin state due to symmetry reasons, the spectra in black and blue in the high-spin state are almost identical. As expected, there is a sudden decrease in  $K_{\beta'}$  intensity when passing the spin-crossover transition. However, note that changes occur over the entire spectrum through the spin-crossover transition which are generally less pronounced when the 3p lifetime broadening is fully taken into account. In the low-spin state, the  $K_{\beta'}$  is not constant, but continues to decrease. In the presence of an exchange field, the lowering of the symmetry allows the coupling between the high- and low-spin states throughout the transition. The XES spectra are calculated for the 10Dq values indicated by the dashed

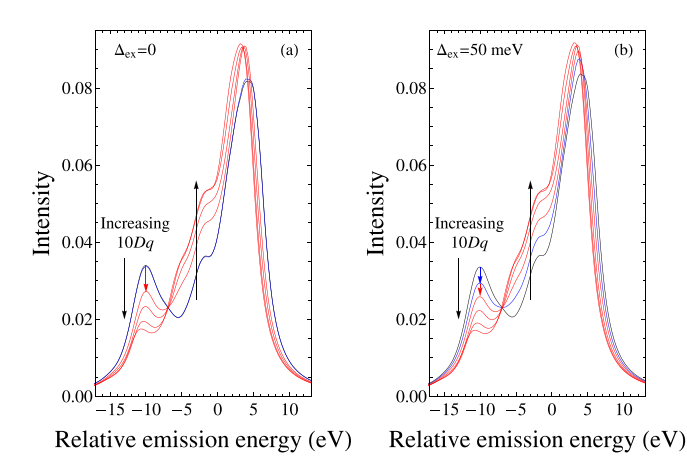


FIG. 4. (a) The  $K_{\beta}$  spectra in the absence of an exchange field  $(\Delta_{\rm ex}=0)$ . The used 10Dq values are indicated by the solid vertical lines in Fig. 3(a). The spectra in black and blue are (predominantly) high spin. The spectra in red are predominantly low spin. (b) The  $K_{\beta}$  spectra in the presence of an exchange field  $(\Delta_{\rm ex}=50\,{\rm meV})$ . The used 10Dq values are indicated by the dashed vertical lines in Fig. 3(a).

vertical lines in Fig. 3(a). The used 10Dq values are slightly higher in energy than those in the absence of the exchange field to account to the shift of the spin-crossover transition. Additionally, the change in 10Dq values around the spin crossover is increased to make the differences more visible. The presence of the exchange field mainly affects the spectra in the high-spin states; see Fig. 4(b). The spectrum in the low-spin state just above the high-to-low spin crossover for  $\Delta_{\rm ex}=0$  is comparable to the spectrum with  $\Delta_{\rm ex}=50$  meV in the middle of the transition. In the low-spin state, the spectra follow a similar trend independent of  $\Delta_{\rm ex}$ .

Although it has been pointed out so far that the  $K_{\beta}$  x-ray emission spectra are significantly more complex than their often relatively simple-looking spectral line shapes suggest, it does not render them useless as a probe of change in the local spin moment. Figure 5 plots the ratio of the  $K_{\beta'}$  and  $K_{\beta_{1,3}}$  integrated intensities. It should be noted that for complex systems, it is not always obvious how to define the  $K_{\beta'}$  region (even for theoretical calculations where the broadening can be varied). Here it is taken as the cluster of states at low emission energies and the cutoff is taken as the local minimum between these states and the rest of the spectrum. Although its definition and their absolute intensity are not trivial, the nature of these states, however complex, still has a very high  $S_F = S - \frac{1}{2}$  character. Therefore, they still reflect changes in the ground-state spin. This is demonstrated in Fig. 5, where the change in integrated intensity of  $K_{\beta'}$  is plotted against the ground-state expectation value of the projected total spin  $S_z$  (in the presence of an exchange field of  $\Delta_{\rm ex}$  = 50 meV). Although not perfect, the  $K_{\beta'}$  intensity follows the trends in  $S_z$ . However, note that the ratios following the S/(S+1) rules should be  $\frac{3}{5}=0.6$  and  $\frac{1}{3}$  in the highand low-spin regions, respectively. The calculated ratios are significantly lower since  $S_F = S - \frac{1}{2}$  character occurs throughout the spectrum, not only in the  $K_{\beta'}$  region.

The calculations done so far were somewhat idealized using a smaller lifetime broadening to highlight the spectral

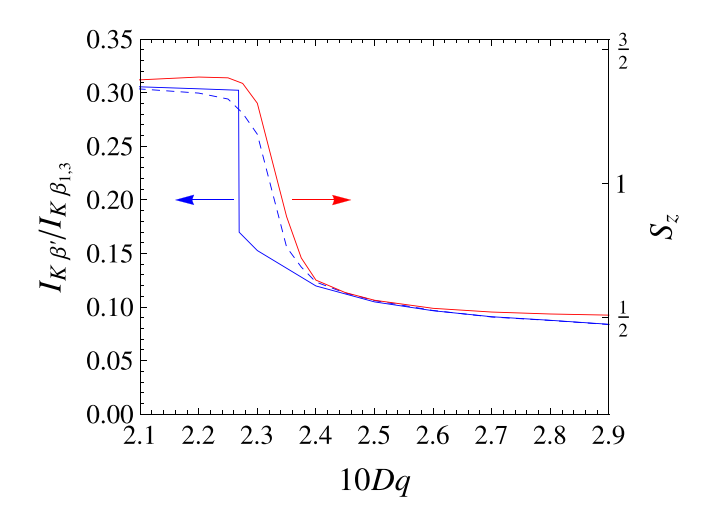


FIG. 5. The intensity ratio of  $K_{\beta'}$  and  $K_{\beta_{1,3}}$  as a function of the octahedral crystal field 10Dq (blue lines) in the absence (solid) and presence (dashed) of the exchange field. The red line shows the ground-state expectation value of the projected total spin  $S_z$  in the presence of the exchange field (red).

features. Figure 6(a) shows a comparison of the experimental data [8] on Na<sub>3</sub>Co<sub>2</sub>SbO<sub>6</sub> and theoretical spectra as a function of pressure. The calculated spectra are shown with a realistic lifetime broadening. The broadening depends on the emission energy. In the  $K_{\beta_{1,3}}$  region, the lifetime broadening is 3.75 eV. The value then increases to over 5 eV in the  $K_{\beta'}$  region. To compare the experimental spectra to the calculations, the pressure needs to be converted into a crystal-field value. The crystal field needs to fit the well-established value at ambient pressure and the value needed for a spin crossover at the correct pressure [8,22]. Under pressure, the effective crystal field increases due to a decrease in cobalt-oxygen distance d, which shows a smooth decline of 10–15% from ambient pressure to 100 GPa. The change in d is taken to follow the behavior of the lattice parameters [8]. The effective crystal field is the combined effect of the larger  $t_{2g}$ - $e_g$  splitting due to hybridization and the increase in the point-charge crystal field. The effective crystal field depends on the lattice parameters as  $(d_0/d)^a$ , where  $d_0$  is the distance at ambient pressure [25]. In order to satisfy these conditions, a value of  $a \cong 5.1$  is needed. This is close to the value of a = 5 expected power for a change in the crystal field due to a change in metal-ligand distance [25].

The experimental spectra in Fig. 6(a) do not show a clear jump in the  $K_{\beta'}$  and are consistent with the calculations in the presence of an exchange field. This conclusion is reinforced by the integrated intensities shown in Fig. 6(b), where no sudden change occurs. Note also that the theoretical width of the transition compares well with the experimental one. This should be compared with the intensity change where the local symmetry is not lowered by the exchange field. Here the integrated intensities show a clear jump, which is not present in the experimental results.

### V. CONCLUSIONS

In this paper, the use of  $K_{\beta}$  x-ray emission to study spincrossover transitions has been evaluated. First, the limitations

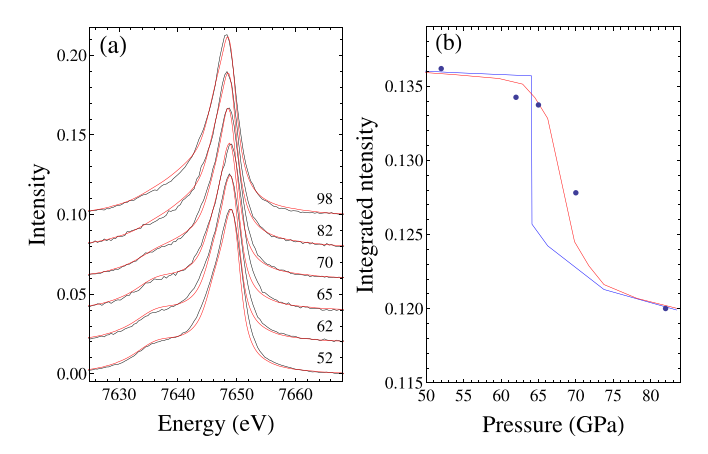


FIG. 6. (a) Comparison of the properly broadened calculated  $K_{\beta}$  spectra with a 50 meV exchange field (red) and experimental data on Na<sub>3</sub>Co<sub>2</sub>SbO<sub>6</sub> (black). The pressures in GPa are indicated in the figure. (b) The dots give integrated intensities over the region from 7631.4 to 7639.2 eV. A comparison is made with the scaled theoretical integrated intensities without (blue) and with (red) an exchange field on the spins.

of Tsutsumi rules [17–19] to predict the absolute intensity of the  $K_{\beta'}$  feature was demonstrated. Although the relative weights of the different spin final states is exact, the intensity of the  $S-\frac{1}{2}$  final states, where S is the ground-state spin, is not restricted to the  $K_{\beta'}$  region. Despite that, the Tsutsumi rule gives a reasonable description of the trends across the transition-metal series and the effects of a spin-crossover transition.

The spin-crossover transition for divalent cobalt has been studied in detail. It is found that the local magnetic moment is stable over a large pressure range. Due to the coupling between the low- and high-spin states, the transition as a function of pressure is not sharp, but broadened by the spinorbit interaction. Even more surprising is the effect of a small exchange field on the interaction. The lowest high-spin state does not couple to the low-spin state in the absence of an exchange field. This gives a jump in the spin. However, in the presence of an exchange field, the transition as a function of pressure is smoothed. In the low-spin state, this smoothing always occurs since the low-spin state does couple to highspin states, albeit not the lowest ones in energy. In addition to the exchange field, other interactions can lower the symmetry in the high-spin state. For example, in systems with a symmetry lower than octahedral, the U' irreducible representation also splits, allowing the coupling between low- and high-spin states. In conclusion, the coupling between low- and high-spin states makes the spin crossover in divalent cobalt significantly more interesting than that in the typical  $d^6$  systems where the change in spin of  $\Delta S = 2$  strongly reduces the coupling between the two spin states.

## ACKNOWLEDGMENTS

Work at Argonne National Laboratory was supported by the U.S. Department of Energy, Office of Science, Office of Basic Energy Sciences, under Contract No. DE-AC02-06CH11357. E.H.T.P. was supported by the U.S. Department of Energy-National Nuclear Security Administration (DOE-NNSA) through the Chicago/DOE Alliance Center (Grant No. DE-NA0004153).

#### DATA AVAILABILITY

The data that support the findings of this article are not publicly available. The data are available from the authors upon reasonable request.

- [1] A. Hauser, Spin Crossover Materials: Properties and Application (Wiley, New York, 2013).
- [2] Spin Crossover in Transition-Metal Compounds, edited by P. Gütlich and H. A. Goodwin (Springer, Berlin, 2004).
- [3] A. Bousseksou, G. Molnár, L. Salmon, and W. Nicolazzi, Molecular spin crossover phenomenon: Recent achievements and prospects, Chem. Soc. Rev. 40, 3313 (2011).
- [4] M. A. Halcrow, Spin-Crossover Materials (Wiley, New York, 2013), pp. i–xviii.
- [5] W. Baker and M. van Veenendaal, Theory of ultrafast photoinduced low-to-high spin crossover in divalent iron systems, Phys. Rev. B 104, 014407 (2021).
- [6] C. Weis, C. Sternemann, V. Cerantola, C. J. Sahle, G. Spiekermann, M. Harder, Y. Forov, A. Kononov, R. Sakrowski, H. Yavaş, M. Tolan, and M. Wilke, Pressure driven spin transition in siderite and magnesiosiderite single crystals, Sci. Rep. 7, 16526 (2017).
- [7] J. Kuneš, A. V. Lukoyanov, V. I. Anisimov, R. T. Scalettar, and W. E. Pickett, Collapse of magnetic moment drives the Mott transition in MnO, Nat. Mater. 7, 198 (2008).
- [8] E. H. T. Poldi, R. Tartaglia, G. Fabbris, N. Nguyen, H. Park, Z. Liu, M. van Veenendaal, R. Kumar, G. Jose, S. Samanta, W. Bi, Y. Xiao, D. Popov, Y. Wu, J.-W. Kim, H. Zheng, J. Yan, J. F. Mitchell, R. J. Hemley, and D. Haskel, Pressure tuning of Kitaev spin liquid candidate Na<sub>3</sub>Co<sub>2</sub>SbO<sub>6</sub>, Commun. Phys. 8, 310 (2025).
- [9] H. Liu, J. Chaloupka, and G. Khaliullin, Kitaev spin liquid in 3d transition metal compounds, Phys. Rev. Lett. 125, 047201 (2020).
- [10] G. Vankó, J.-P. Rueff, A. Mattila, Z. Németh, and A. Shukla, Temperature- and pressure-induced spin-state transitions in LaCoO<sub>3</sub>, Phys. Rev. B **73**, 024424 (2006).
- [11] A. Mattila, J.-P. Rueff, J. Badro, G. Vankó, and A. Shukla, Metal-ligand interplay in strongly correlated oxides: A parametrized phase diagram for pressure-induced spin transitions, Phys. Rev. Lett. 98, 196404 (2007).
- [12] K. Hämäläinen, C.-C. Kao, J. B. Hastings, D. P. Siddons, L. E. Berman, V. Stojanoff, and S. P. Cramer, Spin-dependent x-ray absorption of MnO and MnF<sub>2</sub>, Phys. Rev. B 46, 14274 (1992).

- [13] T. Kachel, C. Carbone, and W. Gudat, Spin polarization of corelevel photoelectrons, Phys. Rev. B 47, 15391 (1993).
- [14] X. Wang, F. M. F. de Groot, and S. P. Cramer, Spin-polarized x-ray emission of 3d transition-metal ions: A comparison via  $K\alpha$  and  $K\beta$  detection, Phys. Rev. B **56**, 4553 (1997).
- [15] G. Vankó, T. Neisius, G. Molnár, F. Renz, S. Kárpáti, A. Shukla, and F. M. F. de Groot, Probing the 3D spin momentum with x-ray emission spectroscopy: The case of molecular-spin transitions, J. Phys. Chem. B 110, 11647 (2006).
- [16] T. Inami, Magnetic circular dichroism in x-ray emission from ferromagnets, Phys. Rev. Lett. 119, 137203 (2017).
- [17] K. Tsutsumi, The x-ray non-diagram lines  $K\beta'$  of some compounds of the iron group, J. Phys. Soc. Jpn. **14**, 1696 (1959).
- [18] K. Tsutsumi and H. Nakamori, X-ray K emission spectra of chromium in various chromium compounds, J. Phys. Soc. Jpn. 25, 1418 (1968).
- [19] K. Tsutsumi, H. Nakamori, and K. Ichikawa, X-ray Mn  $K\beta$  emission spectra of manganese oxides and manganates, Phys. Rev. B **13**, 929 (1976).
- [20] J. Fernández-Rodríguez, B. Toby, and M. van Veenendaal, Xclaim: A graphical interface for the calculation of core-hole spectroscopies, J. Electron Spectrosc. Relat. Phenom. 202, 81 (2015).
- [21] M. van Veenendaal, The Theory of Inelastic Scattering and Absorption of X-rays (Cambridge University Press, Cambridge, 2015).
- [22] M. van Veenendaal, E. H. T. Poldi, L. S. I. Veiga, P. Bencok, G. Fabbris, R. Tartaglia, J. L. McChesney, J. W. Freeland, R. J. Hemley, H. Zheng, J. F. Mitchell, J.-Q. Yan, and D. Haskel, Electronic structure of Co 3d states in the Kitaev material candidate honeycomb cobaltate Na<sub>3</sub>Co<sub>2</sub>SbO<sub>6</sub> probed with x-ray dichroism, Phys. Rev. B 107, 214443 (2023).
- [23] R. D. Cowan, *The Theory of Atomic Structure and Spectra* (University of California Press, Berkeley, 1981).
- [24] J. S. Griffith, *The Theory of Transition-metal Ions* (Cambridge University Press, Cambridge, 1961).
- [25] W. A. Harrison, *Elementary Electronic Structure* (World Scientific, Singapore, 1999).